DOI: 10.1002/ejic.200701356

Sc_3AlN – A New Perovskite

Carina Höglund,*[a] Jens Birch,[a] Manfred Beckers,[a] Björn Alling,[a] Zsolt Czigány,[b] Arndt Mücklich,[c] and Lars Hultman[a]

Keywords: Crystal growth / Density functional theory / Electron microscopy / Perovskite nitride phases / Thin films

Sc_3AlN with perovskite structure has been synthesized as the first ternary phase in the Sc–Al–N system. Magnetron sputter epitaxy at 650 °C was used to grow single-crystal, stoichiometric $Sc_3AlN(111)$ thin films onto MgO(111) substrates with ScN(111) seed layers as shown by elastic recoil detection analysis, X-ray diffraction, and transmission electron microscopy. The Sc_3AlN phase has a lattice parameter of 4.40 Å, which is in good agreement with the theoretically predicted 4.42 Å. Comparisons of total formation energies show that Sc_3AlN is thermodynamically stable with respect to all known binary compounds. $Sc_3AlN(111)$ films of 1.75 µm thickness exhibit a nanoindentation hardness of 14.2 GPa, an elastic modulus of 249 GPa, and a room-temperature electrical resistivity of 41.2 µΩ cm.

Introduction

Perovskites comprise a large family of ternary phases where face-centered non-metallic atoms are added to a metallic body-centered cubic unit cell.[1] Many perovskites have extreme properties, like ferroelectricity,[2] superconductivity[3] even up to 156 K at high pressures,[4] and colossal magnetoresistance.[5] One type of perovskites has a metallic face-centered cubic structure with nitrogen atoms in body-centered position (also known as anti- or inverse perovskites).[6] These materials are interesting due to the possibility to design them as insulators, semiconductors, or conductors depending on their electronic nature.[7,8] Two phases of this kind are Ti_3AlN[9] and Sc_3InN,[10] making Sc_3AlN plausible in the Sc–Al–N system, by replacing Ti by Sc or In by Al, respectively. Here, Al would take cube-corner, Sc face-center, and N body-center positions. However, no ternary phases were reported in the little explored Sc–Al–N system up to now. Known binary phases include the nitrides ScN and AlN as well as the intermetallics $AlSc_2$, AlSc, Al_2Sc and Al_3Sc.[11] Here, we present synthesis and characterization of the new phase Sc_3AlN with perovskite structure, grown as single-crystal thin films by magnetron sputter epitaxy onto MgO(111) wafers with ScN(111) seed layers at a substrate temperature of 650 °C.

[a] Department of Physics, Chemistry and Biology (IFM), Linköping University,
58183 Linköping, Sweden
Fax: +46-13-28-89-18
E-mail: carina@ifm.liu.se
[b] Research Institute for Technical Physics and Materials Science, Hungarian Academy of Sciences,
P. O. Box 49, 1525 Budapest, Hungary
[c] Institute of Ion Beam Physics and Materials Research, Forschungszentrum Dresden-Rossendorf,
P. O. Box 510119, 01314 Dresden, Germany

Results and Discussion

Figure 1 displays the depth-resolved film composition acquired by elastic recoil detection analysis (ERDA) of 60 ± 2 atom-% Sc, 20 ± 1 atom-% Al, and 18 ± 2 atom-% N, hence the aimed Sc/Al/N = 3:1:1 ratios, constant throughout the sampling depth. H, C, and O impurity levels are close to the detection limit, with an average amount <0.5 atom-%.

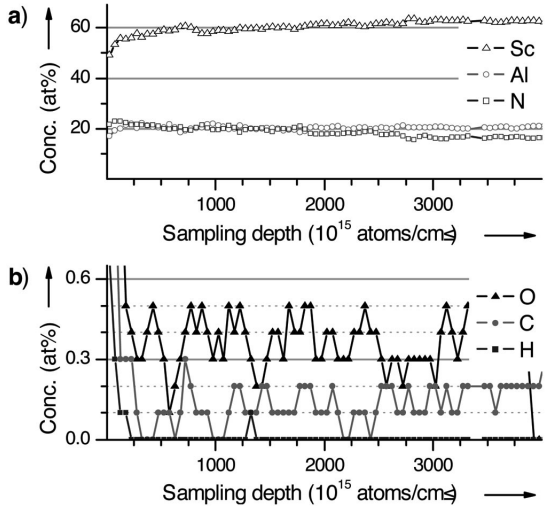

Figure 1. ERDA depth profile from a 1.75 µm thick Sc_3AlN thin film showing the relative amount of (a) Sc (Δ), Al (○), and N (□) and (b) the impurities of O (▲), C (●), and H (■).

The $\theta/2\theta$ X-ray diffraction (XRD) scans from the Sc_3AlN film shown in Figure 2(a) and (b), reveal only the *111* specular reflections from the MgO substrate and the ScN seed layer. These scans as well as pole figures (not shown) indicate a cubic crystal structure for the Sc_3AlN film phase,

with cube-on-cube epitaxy to the substrate and a lattice parameter of 4.40 Å. The non-specular $\omega/2\theta$ scans around the fcc crystal reciprocal lattice points *200*, *220*, and *311* in Figure 2(c) show peaks for each of the Sc_3AlN, ScN, and MgO phases. Corresponding scans around additional perovskite reciprocal lattice points shown in Figure 2(d), however, reveal peaks only from the Sc_3AlN. The relative intensities of the four lowest index perovskite peaks *100*, *210*, *221*, and *300* agree with the structure factors as calculated with the CaRIne crystallography program.

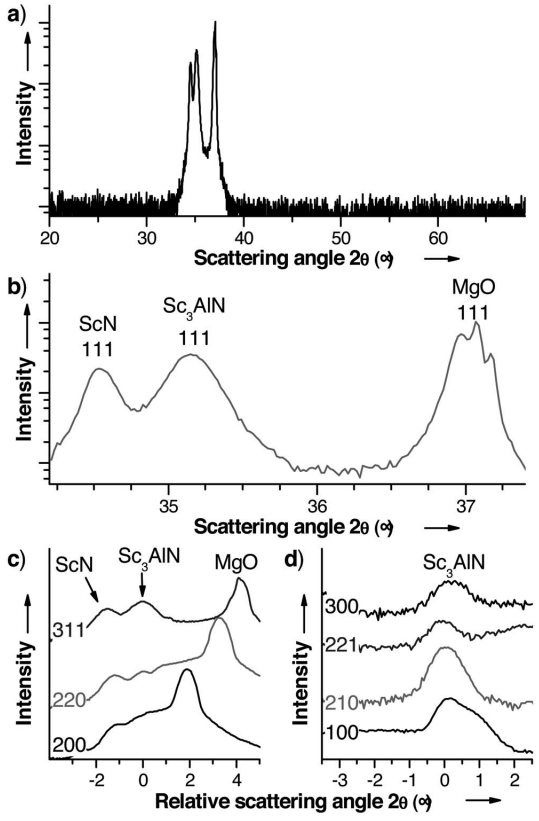

Figure 2. XRD data from a $Sc_3AlN(111)$ film on a MgO(111) substrate with a ScN(111) seed layer recorded as (a) specular $\theta/2\theta$ overview scan, (b) enlarged 111 peaks of (a), and (c) and (d) non-specular $\omega/2\theta$ scans over fcc structure peaks, and additional low index perovskite structure peaks, respectively.

Figure 3(a) shows a cross-sectional transmission electron microscopy (XTEM) image, where the MgO substrate, the ScN seed layer, and the dense Sc_3AlN film are clearly distinguishable. The corresponding selected-area electron diffraction (SEAD) pattern of the film, taken along the $[0\bar{1}1]$ zone axis in Figure 3(b), shows that the film is single-crystalline. The fcc reflections are intense, and the additional perovskite reflections (e.g., *100* and *011*) are weaker, as expected from the structure factors described above. The same appearance of perovskite spots in the SAED patterns was also observed for other low-index zones (not shown). Figure 3(c) displays a high-resolution XTEM image of the Sc_3AlN film along its [210] zone axis. The layered lattice structure observed agrees with the expected perovskite depicted in Figure 3(d), where successive non-equivalent *002* planes consist of Sc and N alternated by Sc and Al. Lattice imaging along the [110], [122], and [123] zone axes yielded the same perovskite structure.

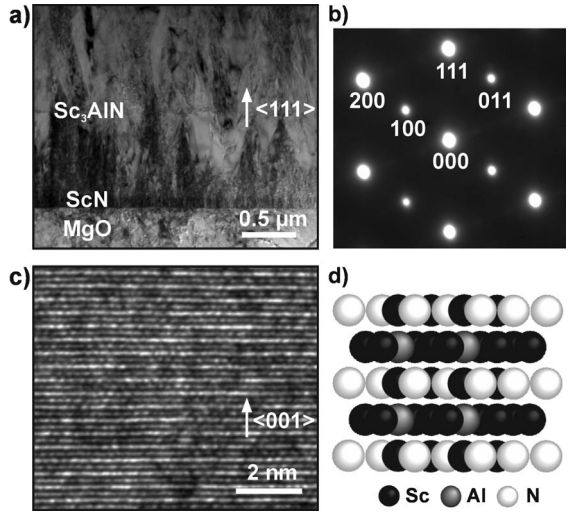

Figure 3. XTEM micrographs from a 1.75 μm thick Sc_3AlN film in (a) overview showing MgO(111) substrate, ScN(111) seed layer, and $Sc_3AlN(111)$ film as well as (b) SAED pattern from the $[0\bar{1}1]$ zone axis of the Sc_3AlN film in (a), (c) C_s-corrected high-resolution XTEM image of the $Sc_3AlN(111)$ film in the [210] zone axis, and (d) the perovskite structure corresponding to (c).

Both SAED and XRD data yield a lattice constant of 4.40 Å, which is in excellent agreement with the calculated equilibrium lattice parameter for perovskite Sc_3AlN of 4.42 Å. The difference of ca. 0.5% is within the accuracy of the method, as the applied GGA functional is known to slightly overestimate lattice parameters. For comparison, also the lattice parameters of Ti_3AlN and Sc_3InN were calculated using the same procedure, giving values of 4.11 Å and 4.48 Å to be compared with experimental values of 4.11 Å[9] and 4.45 Å,[10] respectively.

Thermodynamic stability of the perovskite Sc_3AlN at the global concentration of Sc/Al/N = 3:1:1 requires that the free energies are:

$$G(Sc_3AlN) < G(ScN) + G(AlSc_2) \quad (1)$$

$$G(Sc_3AlN) < G(AlN) + 3G(Sc) \quad (2)$$

The total enthalpy calculated for the optimal volume for each compound yields:

$$E(Sc_3AlN) - E(ScN) - E(AlSc_2) = -0.535 \text{ eV} \quad (3)$$

$$E(Sc_3AlN) - E(AlN) - 3E(Sc) = -2.603 \text{ eV} \quad (4)$$

Since the entropy contribution to the total free energies is likely to be insignificant for the binary line compounds at the moderate temperatures of our experiments, we conclude that the perovskite Sc_3AlN is thermodynamically stable. Films deviating from optimal Sc/Al/N = 3:1:1 stoichiometry with increased Al and N content were also deposited. The initial results show that the Sc_3AlN perovskite under such condition is a line compound in equilibrium with ScN and Al_3Sc at 650 °C, and with ScN and Al_2Sc at higher temperatures.

Nanoindentation experiments of a stoichiometric 1.75 μm thick $Sc_3AlN(111)$ film with a ScN(111) seed layer on MgO(111) yield a hardness of 14.2 GPa and an elastic modulus of 249 GPa. These values are lower than for ScN with a reported hardness of 21 GPa and elastic modules of 356 GPa,[12] but in close range of the related perovskite Ti_3AlC with values of 11 GPa and 240 GPa, respectively.[13]

Electrical resistivity measurements of the same $Sc_3AlN(111)$ film yields a room-temp. sheet resistance R_s = 235 mΩ and resistivity ρ = 41.2 μΩcm. The films exhibit metallic conductivity as inferred from a linear increase in resistivity over the range of 100–272 K, with a temperature coefficient of 1.743×10^{-3} K^{-1}.

Conclusions

The perovskite structure Sc_3AlN has been synthesized by magnetron sputter epitaxy as the first ternary phase in the Sc–Al–N system. Sc_3AlN has a lattice parameter of 4.40 Å, a hardness of 14.2 GPa, an elastic modulus of 249 GPa, and a room-temp. resistivity of 41.2 μΩcm.

Experimental Section

The deposition experiments were performed in an ultra-high-vacuum chamber at a base pressure of 1.33×10^{-6} Pa. Reactive sputtering from unbalanced type II magnetrons with 50-mm diameter Sc and 75-mm Al elemental targets was used to epitaxially grow 100-nm ScN(111) seed layers followed by up to 1.75 μm thick $Sc_3AlN(111)$ films onto polished $10 \times 10 \times 0.5$ mm MgO(111). Prior to deposition, the substrates were cleaned in ultrasonic baths of trichloroethylene, acetone and 2-propanol and blown dry in dry N_2. This was followed by degassing in the chamber at 900 °C for 1 h before ramping down to the deposition temperature of 650 °C, controlled by a thermocouple positioned behind the substrate and calibrated by pyrometry. During deposition, the Ar partial pressure was kept at 1.064 Pa, while the N_2 partial pressure was 0.04 and 0.03 Pa for ScN and Sc_3AlN depositions, respectively. The substrate potential was set to be floating. The magnetron power of Sc for ScN was set to 200 W, and the powers for Sc_3AlN were 250 W and 70 W for Sc and Al, respectively. The film composition was determined by elastic recoil detection analysis, using a 40 MeV $^{127}I^{9+}$ beam at 67.5° incidence and 45° scattering angle, and evaluated with the CONTES code.[14] The crystal structure was characterized by Cu-K_α X-ray diffraction using a Philips X'Pert 4-axis diffractometer in low-resolution mode and a Philips Bragg–Brentano diffractometer. Cross-sectional transmission electron microscopy was carried out with FEI Tecnai G^2 TF 20 UT FEG and C_s-corrected FEI TITAN FEG microscopes operated at 200 kV and 300 kV, respectively. Nanoindentation at a maximum load of 7 mN was performed in a Hysitron Triboscope equipped with a Berkovich tip. The electrical resistivity as a function of temperature was determined using a van der Pauw setup,[15] with four electrical contact points applied in a 4.5×4.5 mm square. The contacts consisted of Cr and Au bond pads evaporated onto Pt anchors prepared by focus ion beam. First-principles calculations were carried out within a density functional theory framework for the proposed Sc_3AlN perovskite structure as well as for all known competing binary phases. The projector augmented wave method as implemented in the Vienna ab-initio simulation package[16,17] was used together with the generalized gradient approximation (GGA)[18] for the exchange-correlation functional.

Acknowledgments

We acknowledge the financial support given by the Swedish Research Council (VR), the Swedish Foundation for Strategic Research (SSF) Center on Materials Science for Nanoscale Surface Engineering (MS^2E) and the Knut and Alice Wallenberg Foundation. We also acknowledge assistance by Jens Jensen at the Tandem Laboratory, Uppsala University for ERDA, Finn Giuliani for nanoindentation and FIB, and Anita Lloyd Spetz and Mike Andersson for wire-bonding preparation.

[1] G. Rose, *Ann. Phys. Chem.* **1839**, *48*, 551–572.
[2] A. von Hippel R. G. Breckenridge, A. P. de Bretteville, Jr., J. M. Brownlow, F. G. Chesley, G. Oster, L. Tisza, W. B. Westphal, *NRDC Report* **1944**, no. 300.
[3] A. W. Sleight, J. L. Gillson, P. E. Bierstedt, *Solid State Commun.* **1975**, *17*, 27–28.
[4] S. N. Putilin, E. V. Antipov, M. Marezio, *Physica C* **1993**, *212*, 266–270.
[5] R. von Helmolt, J. Wecker, K. Samwer, K. Bärner, *J. Magn. Magn. Mater.* **1995**, *151*, 411–416.
[6] J. Jäger, D. Stahl, P. C. Schmidt, R. Kniep, *Angew. Chem. Int. Ed. Engl.* **1993**, *32*, 709–710.
[7] M. Y. Chern, D. A. Vennos, F. J. DiSalvo, *J. Solid State Chem.* **1992**, *96*, 415–425.
[8] R. Niewa, W. Schnelle, F. R. Wagner, *Z. Anorg. Allg. Chem.* **2001**, *627*, 365–370.
[9] J. C. Schuster, J. Bauer, *J. Solid State Chem.* **1984**, *53*, 260–265.
[10] M. Kirchner, W. Schnelle, F. R. Wagner, R. Niewa, *Solid State Sci.* **2003**, *5*, 1247–1257.
[11] T. B. Massalski in *Binary Alloy Phase Diagrams*, ASM International, Metals Park, Ohio, **1986**, vol. 1, p. 162.
[12] D. Gall, I. Petrov, N. Hellgren, L. Hultman, J. E. Sundgren, J. E. Greene, *J. Appl. Phys.* **1998**, *84*, 6034–6041.
[13] O. Wilhelmsson, J. P. Palmquist, E. Lewin, J. Emmerlich, P. Eklund, P. O. Å. Persson, H. Högberg, S. Li, R. Ahuja, O. Eriksson, L. Hultman, U. Jansson, *J. Cryst. Growth* **2006**, *291*, 290–300.
[14] M. S. Janson in *CONTES, Conversion of Time-Energy Spectra – a Program for ERDA Data Analysis*, Uppsala University, **2004**, internal report.
[15] L. J. van der Pauw, *Philips Res. Rep.* **1958**, *13*, 1–9.
[16] P. E. Blöchl, *Phys. Rev. B* **1994**, *50*, 17953–17979.
[17] G. Kresse, J. Hafner, *Phys. Rev. B* **1993**, *48*, 13115–13118; G. Kresse, J. Hafner, *Phys. Rev. B* **1994**, *49*, 14251–14269.
[18] J. Perdew, K. Burke, M. Ernzerhof, *Phys. Rev. Lett.* **1996**, *77*, 3865–3868.

Received: December 18, 2007
Published Online: January 30, 2008

